ISSN (Print) 1226-1750
ISSN (Online) 2233-6656
Journal of Magnetics 22(3), 414-422 (2017) https://doi.org/10.4283/JMAG.2017.22.3.414

Analysis of Half Halbach Array Configurations in Linear Permanent-Magnet Vernier Machine

Fangfang Bian[1,2], Wenxiang Zhao[1,2]*, Jinghua Ji[1,2], and Liang Xu[1,2]

[1]*School of Electrical and Information Engineering, Jiangsu University, Zhenjiang 212013, China*
[2]*Jiangsu Key Laboratory of Drive and Intelligent Control for Electric Vehicle, Zhenjiang 212013, China*

(Received 7 April 2017, Received in final form 15 June 2017, Accepted 20 June 2017)

Due to the high efficiency, high force capability and low cost, the linear permanent-magnet (PM) vernier (LPMV) machine is very suitable for long stroke applications such as urban rail transits. This paper proposes the LPMV machines with various topologies of half Halbach PM array, and investigates their electromagnetic performances, such as back electromotive force, force capability, PM eddy current loss and iron loss. Firstly, the configuration and operation principle of the LPMV machines are presented. By using the finite element method, it can be known that the LPMV machine with half Halbach PM array in the armature core exhibits high thrust and low detent force. Then, the demagnetizations of half PM array are analyzed to guarantee the security and credibility of the machine in operation. Finally, the effectiveness of the theoretical analysis is validated by the experiments on a prototype of the LPMV machine.

Keywords : Permanent-magnet machine, linear machine, vernier structure, half Halbach array, magnetizing angle

1. Introduction

The permanent-magnet (PM) vernier (PMV) machine, which can offer simple mechanical structure, sinusoidal back electromotive force (back-EMF), and high torque density, belongs to the class of stator-PM machines. Unlike other PM machines, PMV machines operate based on the magnetic gear flux field modulation [1-7]. A small displacement between the rotor and stator of PMV machines causes a great change on flux, resulting in the generation of high torque. Therefore, the PMV machine has been regarded as an excellent candidate in high torque application.

In 1995, Ishizak firstly proposed the PMV machine. Then, Kim and Lipo accurately derived the fundamental back-EMF and power equations, and analyzed the main factors that affected the torque of PMV machine [8]. In [9], the magnetic geared PMV machine and the regular PM machine were compared, showing that the back-EMF waveform of magnetic geared PMV machine was more sinusoidal than that of the regular PM machine. In order to maximize the torque, Toba and Lipo studied comprehensive design considerations of the surface PMV machine [1]. Meanwhile, many PMV topologies were proposed to further improve the torque density, such as the integral and fractional slot PMV machines [6], surface-mounted double rotor PMV machine [10], yet they suffered from relatively low ratio of torque to PM usage. These drawbacks were improved by the modular three-phase PMV machine with consequent-poles [11], and toroidal-winding outer-rotor PMV machine [12]. In addition, the torque density of PMV machine was also increased by employing the spoke and interior magnets [4, 13].

Usually, the appearance of a new rotary electrical machine can result in the descendant of a new linear machine accordingly. The linear PMV (LPMV) machines are classified into two types by the flux modulation method in the air-gap region. Namely, one is the linear vernier hybrid machine, and the other is called as the primary LPMV machine, which has flux modulation poles on the stator and the surface-mounted PMs on the mover [14, 15]. In [16] and [17], the horizontal magnetized PMs were added to form a new half Halbach PM array which could reduce the fringing leakage flux and enhance the thrust force capability of the LPMV machine. However, the configuration of the half Halbach PM array is still lack in the thorough research.

*Corresponding author: Tel: +86-511-887787773
Fax: +86-511-887787773, e-mail: zwx@ujs.edu.cn

The purpose of this paper is to design and investigate the different topologies of half Halbach PM arrays in one LPMV machine. The irreversible demagnetization of half Halbach PM array in LPMV machine will result in serious degradation of electromagnetic performance, such as the decreases of back-EMF, torque density, power and efficiency. Therefore, it is necessary to consider the demagnetization condition to ensure the safe operation of the machine. The configuration and operation principle will be described in Section II. In Section III, the influences of key parameters of half PM array will be assessed by using the finite element method (FEM) on back-EMF, force capability and loss. The irreversible demagnetization of optimal half PM array will be studied in Section IV. To verify the theoretical and FEM results, a LPMV prototype with one half PM array is built and tested in Section V. Finally, the conclusion will be drawn in Section VI.

2. Configuration and Operation Principle

2.1. Configuration

Figure 1 shows the configuration of the LPMV machine in which the stator is designed as simple iron core with salient teeth. The mover consists of laminated iron cores with three-phase armature windings and half PM arrays embedded in the virtual slots. It has a similar structure compared to its counterparts [16, 17], except the topologies of half PM array to reduce the leakage flux around PMs and improve the air gap flux density. This machine is particularly attractive for long stroke applications such as urban rail transits. Its PM materials and armature windings can be set in the train, while the long rail is composed of irons, hence improving efficiency and reducing cost.

Half Halbach PM array can be accomplished by the segmentations of PMs. The choices of the numbers of segments per pole (NSPP) are based on following considerations. First, the high NSPP will result in the sinusoidal air gap flux density [18]. Thus, the NSPP are firstly chosen as 2, 3 and 4. Second, the space for the half PM array in this LPMV machine is limited. If the NSPP is equal to 4, the increases of the cost and difficulty are particularly significant for that the mover has a large number of magnets with specific magnetizing directions [19]. When taking into account these considerations holistically, a trade-off has to be made. Therefore, in the proposed half PM arrays, the NSPP are chosen as 2 and 3. The compromised NSPP in the LPMV machine are adopted by using the half PM array of three magnets

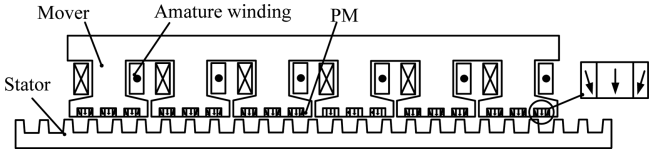

Fig. 1. Configuration of LPMV machine.

whose magnetizing directions are illustrated by the arrows in Fig. 1. The vertically magnetized PM is sandwiched between the other two PMs in one half PM array. As the vertically magnetized PM is removed, it is equal to the case that the proposed half PM array has two magnets.

In general linear machines, the magnetizing angle of each PM segment is obtained by the analytical model, thus the near-sinusoidal air gap flux density distribution can be generated. Since the special constructions of the half PM arrays, this method cannot be fully utilized here. Thus, the FEM method will be used in this work to study the performances of the LPMV machine. Based on the combinations of different magnetizing angle and pole-arc ratio of each magnet, more magnetic fluxes produced by the half PM arrays can be distributed in the air-gap side due to the superposition effect [18-20].

2.2. Operation Principle

Since the LPMV machine is one of the primary PM machines with magnetic gear effect, its operation principle is similar to that of the conventional PMV machines and the magnetic gear [16, 17]. The stator teeth modulate the PM magnetic field to produce the effective magnetic field. The pole-pair number of the PM magnetic field is p_{PM}, the number of stator teeth is p_s and the pole-pair number of the fundamental component of the air-gap magnetic field modulated by the PMs and the stator teeth is p_w. Thus, the relationship among p_{PM}, p_s and p_w is governed by

$$p_w = |p_{\mathrm{PM}} - p_s| \tag{1}$$

$$v_w = \frac{p_s}{p_w} v_s \tag{2}$$

$$G = \frac{p_s}{p_w} \tag{3}$$

where v_s and v_w are the speeds of the stator and the effective flux in the armature windings, respectively, and G is the so-called magnetic gear ratio. Therefore, the speed of the effective flux is G times that of the stator. So, the thrust force can be improved.

Hence, the induced phase EMF amplitude E_{ph} can be deduced as

$$E_{\text{ph}} = \frac{2k_w c_s N N_s B_{w\max} l_m G v_s}{k_d} \tag{4}$$

where k_w and k_d are the phase winding factor and flux leakage factor, respectively, c_s is the pole arc coefficient of the stator teeth, $B_{w\max}$ is the amplitude of effective flux density, N and N_s are the number of turns per coil and the number of coils per phase, respectively, l_m is the mover width . On the other hand, the phase current amplitude I_{am} can be expressed as

$$I_{\text{am}} = \frac{\sqrt{2} A_s l_a}{2mNN_s} \tag{5}$$

where A_s, l_a and m are the electric loading, the length of the mover and the number of phase, respectively. Therefore, the out power P and electromagnetic force F of the LPMV machine can be given by [21]

$$P = \frac{\sqrt{2}}{2} \frac{k_w c_s A_s B_{w\max} l_m l_a G v_s}{k_d} \tag{6}$$

$$F = \frac{\sqrt{2}}{2} \frac{k_w c_s A_s B_{w\max} l_m l_a G}{k_d} \tag{7}$$

It can be seen that electromagnetic force is in direct proportion to the amplification factor of the magnetic gear G. The LPMV machine can offer the high force density as long as the multiply between $B_{w\max}$ and G is large enough.

3. Influences of Key Parameters of Half HALBACH PM array

The basic parameters of the LPMV machine are listed in Table 1. To facilitate the understanding of half PM array, the design dimensions and a referenced coordinate system are illustrated in Fig. 2 and Fig. 3, respectively.

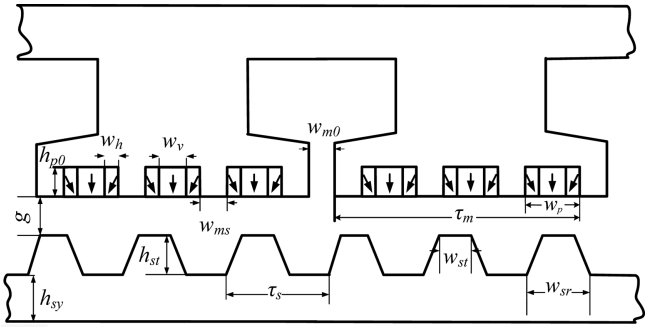

Fig. 2. Design dimensions.

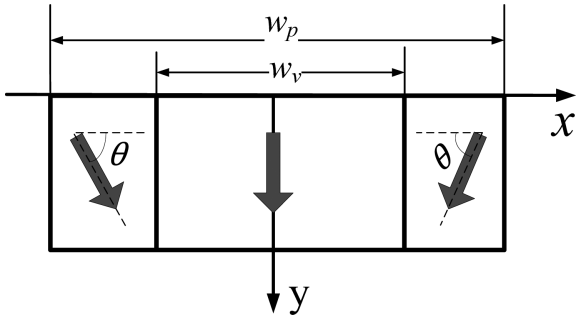

Fig. 3. One half PM array.

Namely, the angle between the PMs on both sides and the X axis is defined as magnetizing angle θ, and the ratio between the widths of the vertically magnetized PM and single half PM array is defined as $c_w = w_v/w_p$. Due to the symmetric structure of side-PMs, the definite of c_w means the pole-arc ratio of horizontal PM segment is specified. By changing the two parameters, different topologies of half PM arrays can be designed. This section will investigate the influences of these arrays on back-EMF, thrust force and loss.

Considering the mach inability and strength of the LPMV machine, the feasible values of c_w are designed as

Table 1. Design specifications of LPMV machine.

Rated power (W)	518	Rated speed, v_s (m/s)	1.5
Rated Current (A)	5	Force density (N/m^3)	1.4×10^5
Current density, J (A/mm^2)	3.3	Rated voltage (V)	270
Armature windings per coil, N	100	Series coils per phase, N_s	2
Copper loss (W)	48.6	Mover width, l_m (mm)	120
Mover pole pitch, τ_m (mm)	49	Stator pole pitch, τ_s (mm)	14.7
Mover slot opening, w_{m0} (mm)	2	Stator tooth tip, w_{st} (mm)	5.2
Mover high, h_m (mm)	50	Stator tooth root, w_{sr} (mm)	5.7
Mover yoke high, h_{my} (mm)	15	Stator tooth height, h_{st} (mm)	8
Mover spilt tooth width, w_{ms} (mm)	5	Air gap length, g (mm)	2
PM high, h_{P0} (mm)	5	Magnetizing angle, θ (°)	0~90
Horizontally magnetized PM width, w_h (mm)	2~4.5	PM volume (mm^3)	9.72×10^4
PM material	N35H	Magnet remanence, B_i (T)	1.2 (20°C)

5/9, 4/9, 1/3, 2/9 and 0. The magnetizing angle θ can range from 0° to 90°. When the LPMV machine operates at 1.5 m/s, its no-load and on-load performances are investigated as follows. In order to take into account magnetic saturation during the analysis, the permeability of back irons is based on practical data of iron materials.

3.1. Magnetic Field Distributions

Since the number of pole-pair p_{PM} and p_s are respectively equal to 18 and 20, the effective magnetic field having 2 pole-pair in the LPMV machine can be modulated for magnetic coupling to achieve energy conversion. The field distributions of one pole-pair under no-load operation are shown in Fig. 4, which includes the topologies of the half PM arrays when the values of θ are selected as 0°, 30°, 60° and 90°, respectively. It is obvious that the fluxes in red solid loop is reduced initially and then increased as the increase of the angle θ, thus verifying that the various horizontal component of one half PM array has the significant influence on the machine performance. Moreover, when the angle θ is equal to 30°, as shown in Fig. 4(b), the fluxes in the red dotted loop between the half PM array and the core is minimum compared with its counterparts in Figs. 4(a), 4(c) and 4(d).

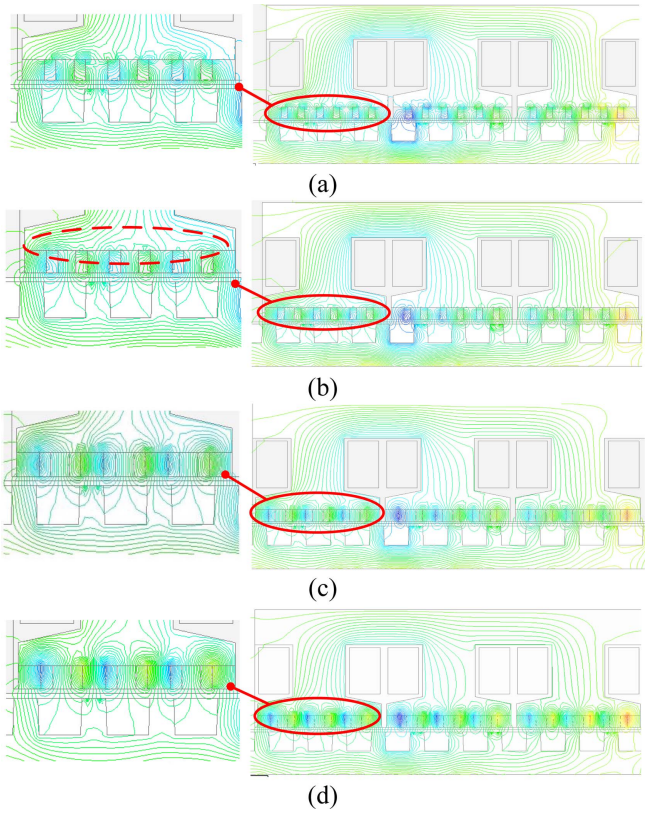

Fig. 4. (Color online) No-load magnetic field distributions. (a) 0°. (b) 30°. (c) 60°. (d) 90°.

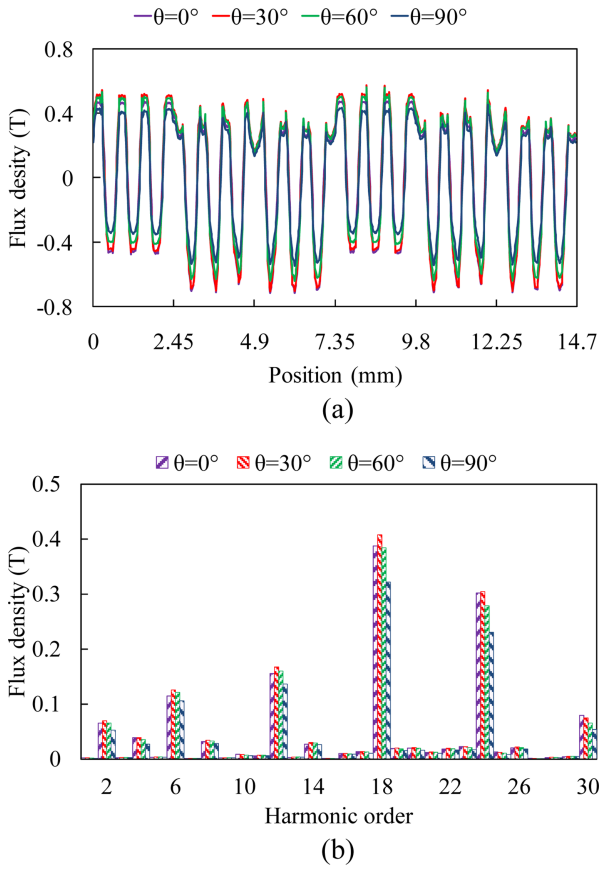

Fig. 5. (Color online) Air gap flux density. (a) Waveforms. (b). Harmonic analysis.

In the foregoing analysis, the various topologies of half PM arrays can improve the air gap flux density due to the self-shielding characteristics. It is confirmed by the corresponding amplitudes of flux densities in Fig. 5(a). The air gap flux densities have a large number of harmonics, as shown in Fig. 5(b). It is clear that the magnetic field harmonics not only contain the effective air-gap magnetic field with 2 pole-pair. Also, it includes the 18 pole-pair harmonic produced by the half PM arrays. The harmonic components with 6, 12 and 24 pole-pair exist due to the modulations between the PMs and teeth. In this case, 6th, 12th, 18th and 24th flux harmonics are stationary and do not induce back-EMF in the coils. The 2th harmonic is the working flux harmonic which can produce fundamental back-EMF and contribute to torque transmission in the air gap.

3.2. Back-EMF

The back-EMF is an important criterion when evaluating the performance of one machine. Figure 6 compares the back-EMF with different values of magnetizing angle θ and ratio c_w. It is obvious that as the angle of θ

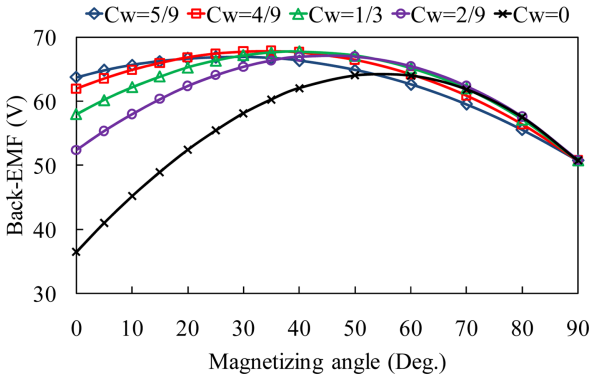

Fig. 6. (Color online) Fundamental amplitudes of the back-EMF at no-load.

increases, the fundamental amplitude of the back-EMF rapidly increases initially, and then gradually reduces. It is because that the horizontal component which plays the role of congregate effect is reduced when the angle of θ exceeds a certain critical value. Furthermore, the point of optimum magnetizing angle θ moves right as the decrease of the ratio c_w. On the other hand, it is shown that the greatest back-EMF fundamental amplitudes with different values of c_w and θ are nearly equal to each other.

3.3. Thrust Force and Detent Force

When $i_d = 0$ is adopted, the average thrust force are shown in Fig. 7 in which three phase armature windings are excited with the 5 A sinusoidal current. It can be found that the force versus angle waveforms vary consistently with that of back-EMF. It is because that their amplitudes are both proportional to B_{wmax}.

Detent force is one of the most annoying problems in linear PM machines. The detent force can cause the thrust ripple K_F which is defined in (8), so it is necessary to minimize the detent force for the smooth motion of the machine.

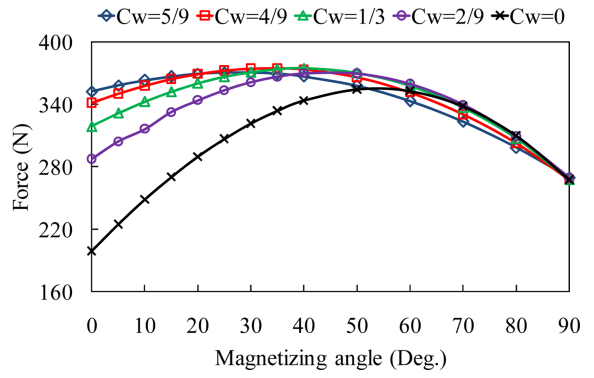

Fig. 7. (Color online) Thrust force at rated operation.

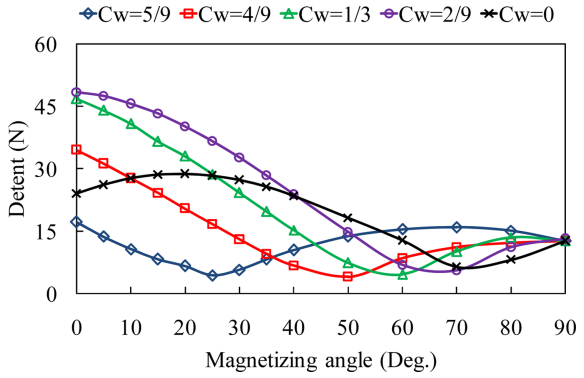

Fig. 8. (Color online) Detent force.

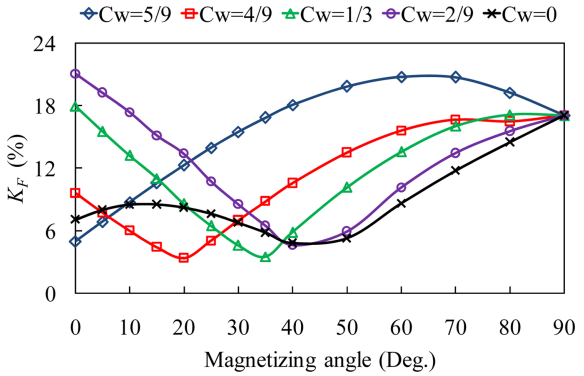

Fig. 9. (Color online) Force ripple.

$$K_F = \frac{F_{\max} - F_{\min}}{F_{\text{ave}}} \times 100\% \tag{8}$$

where the $F_{\max}$, $F_{\min}$, and F_{ave} are the maximum, minimum and average amplitudes of the thrust force, respectively.

Figure 8 shows that the detent force decreases to minimum initially and then increases. As can be seen, the detent forces versus magnetizing angle θ curves are presented the contradictory trends with the ones of thrust force. It means that the LPMV machine can achieve the high average thrust force as well as the low force ripple based on the appropriate combination of the magnetizing angle θ and the ratio c_w. The relationship between the thrust ripple and θ is also reported in Fig. 9.

3.4. Loss

Figure 10 shows the PM eddy current and iron losses of the LPMV machine with various half PM array topologies. It can be seen that the PM eddy current loss change significantly with the variation of c_w. When the ratio c_w decreases to 1/3 and 2/9, the PM eddy current loss is not obviously reduced.

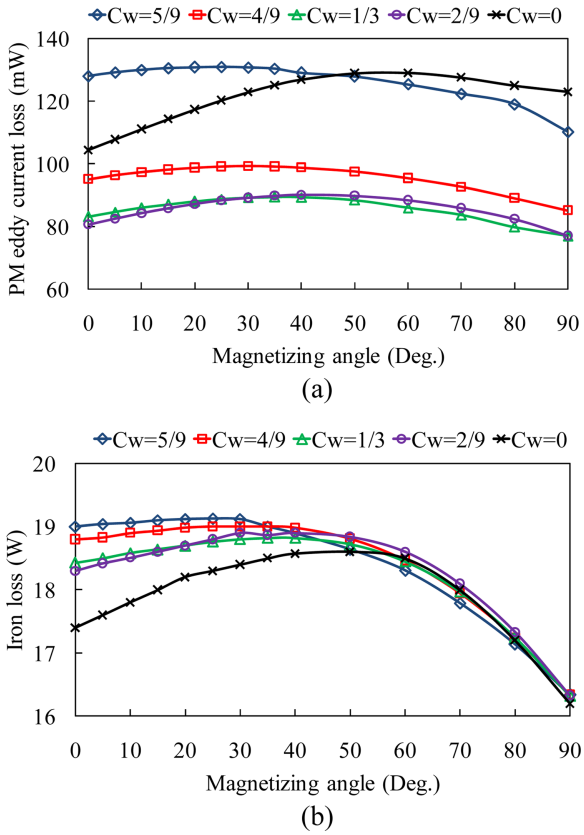

Fig. 10. (Color online) Loss at rated operation. (a) PM eddy current loss. (b) Iron loss.

Furthermore, as the NSPP is equal to 2, the PM eddy current loss increases initially, and then gradually reduces. The influence to the iron loss is also shown in Fig. 10(b).

It is from the analysis above-mentioned that good electromagnetic characteristics of the LPMV machine can be provided when the values of c_w are designed as 5/9, 4/9, 1/3, 2/9 and 0, the optimal points of magnetizing angle θ are chosen as 0°, 25°, 35°, 50° and 50°, respectively. The five cases have the advantages of higher thrust force and smaller pulsation than other combinations.

4. Demagnetization Analysis

Although the electromagnetic characteristics of these combinations are investigated, the issue of demagnetization has not yet been addressed. It is necessary to analyze the demagnetization performance to ensure the half PM arrays of the five combinations can withstand heavy load or fault conditions. In this work, the critical irreversible demagnetization of the half PM array in the LPMV machine occurs when the flux density is below the assumed point 0 T. In addition, the operating temperature has been found to have influence on the demagnetization, thus the temperature of half PM array is kept to the constant of 70°C.

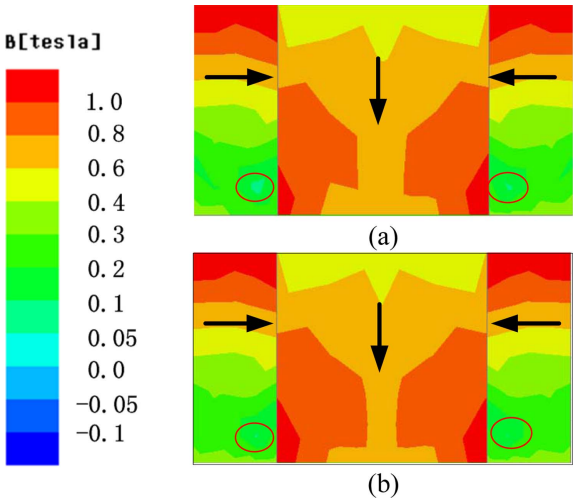

Fig. 11. (Color online) Flux density distributions at no-load. (a) Unaligned position. (b) Aligned position.

4.1. Self-demagnetization

To investigate the self-demagnetization of the half PM array, the LPMV machine operates at no-load. Figure 11 illustrates the flux density distributions of one half PM array in which the arrows represent the PMs magnetizing directions. It can be noticed that near the air gap, the left and right corners (in the red solid circle) of the half PM array are vulnerable to demagnetized when the mover split tooth is not aligned with the stator pole [22, 23]. It is caused by the flux leakage between the half PM arrays and mover split teeth. The directions of flux lines flowing through the bottom part of side-PMs are opposite to the ones of PMs. When the mover shifts left versus the stator, the left corner near the air gap is more susceptible to partial demagnetization than that of the right one. Until the moment that the mover virtual tooth is aligned with the stator pole, the self-demagnetization effect will be symmetric and lowered because the dominant flux will pass through the stator poles, as shown in Fig. 11(b).

4.2. Demagnetization Due to Armature Reaction

The analysis of demagnetization due to armature reaction has been made by the magnetic equivalent circuit model and verified by FEM in [22]. Thus, the demagnetization due to armature reaction can be discussed when the armature windings are excited with sine currents and the PMs are not magnetized. The risk of demagnetization is greatest when the machine operates at the maximum current loading. Figure 12 shows the flux distribution (the mover is symmetrical in structure and only half of the

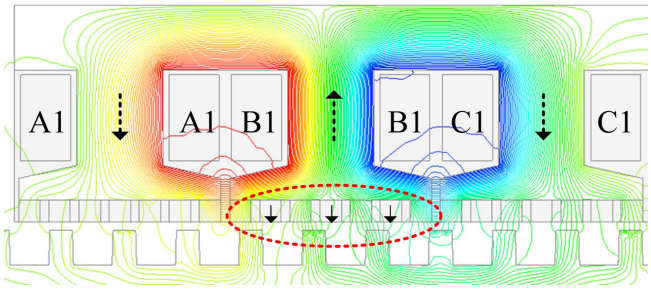

Fig. 12. (Color online) Flux distribution under armature reaction.

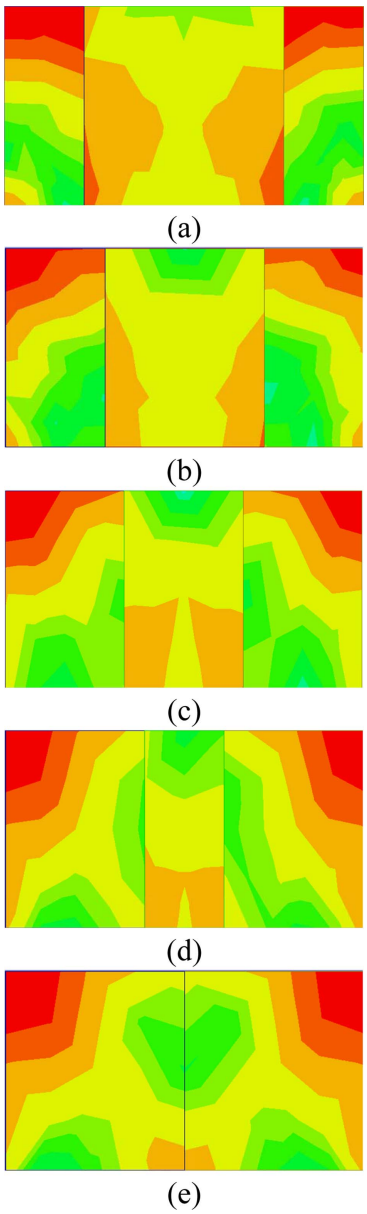

Fig. 13. (Color online) Flux density distributions. (a) $c_w = 5/9$, $\theta = 0°$. (b) $c_w = 4/9$, $\theta = 25°$. (c) $c_w = 1/3$, $\theta = 35°$. (d) $c_w = 2/9$, $\theta = 50°$. (e) $c_w = 0$, $\theta = 50°$.

distribution is shown for simplicity) while the winding B1 is excited with the large positive current. The arrows in black dotted lines and solid lines represent the flux directions and the magnetizing directions of PMs, respectively. As the phase current is at the maximum, the mover virtual tooth is not aligned with the stator pole, thus avoiding the serious demagnetizations of the vertically magnetized PMs. The fluxes pass through the split teeth as well as the side-PMs, resulting that the more susceptible demagnetized positions occur in the left corners of the half PM arrays.

4.3. Overall-demagnetization

To evaluate the demagnetization performance of the LPMV machine, the three phase windings are set to three times the rated current in the simulation. The LPMV machine runs for one full electrical cycle under this overload condition. The flux density distributions at unaligned position are presented in Fig. 13. As can been seen, owe to the superposition of self-demagnetization and demagnetization due to the armature action, the most likely demagnetization areas are still in the corners of the half

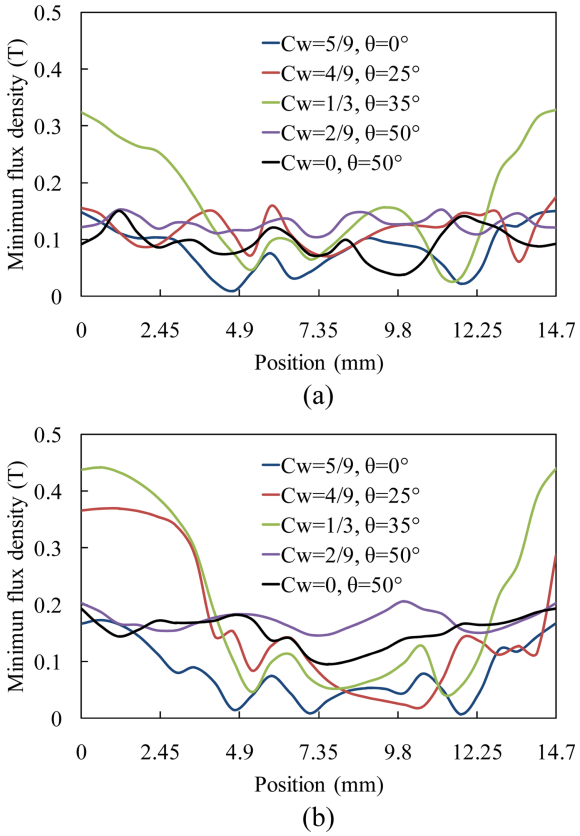

Fig. 14. (Color online) Minimum flux densities versus mover positions. (a) The left corner of the half PM array. (b) The right corner of the half PM array.

PM arrays near the air gap. When the ratio of c_w decreases, the top of the vertically magnetized PM appears the certain possibility of demagnetization. The minimum flux densities of the left and right PMs versus the mover positions are shown in Fig. 14. By analyzing the demagnetization performances, it can be noted that five combinations of the half PM arrays possess the strong capability of withstanding the possible irreversible demagnetization.

5. Experimental Analysis

Considering the process and the existing equipment, the LPMV prototype machine with $c_w = 5/9$, $\theta = 0$ has been built to validate the theoretical analysis, as shown in Fig. 15(a).

In Fig. 15(b), a force sensor is fixed at the top of the mover to measure the thrust force of the prototype machine, and a grating ruler is provided on the side to measure the displacement of the mover. The whole drive control system is based on a digital signal processing unit-TMS320F2812, and a three-phase integrated power module.

The no-load back-EMF waveforms and harmonics are measured in Fig. 16. The insignificant difference between the experimental (54 V, 1.5 m/s) and simulation results (64 V, 1.5 m/s) is caused by the measurement and manufacture, so the simulation results exhibit a good agreement

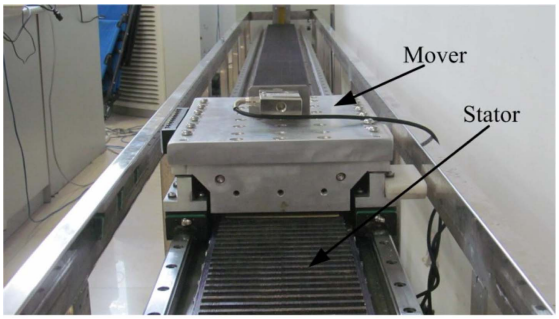

(a)

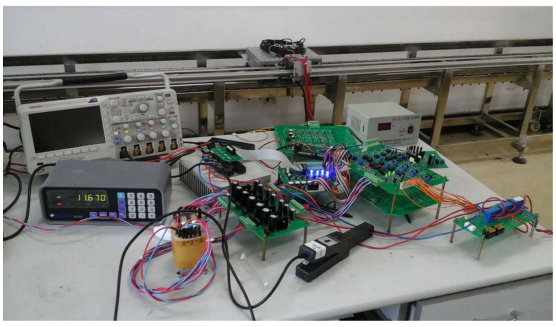

(b)

Fig. 15. (Color online) Prototype of LPMV machine. (a) Machine. (b) Control platform.

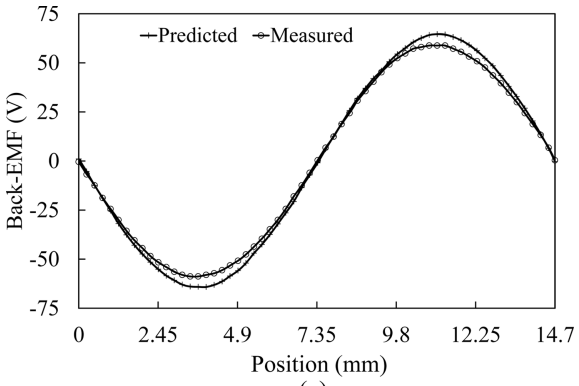

(a)

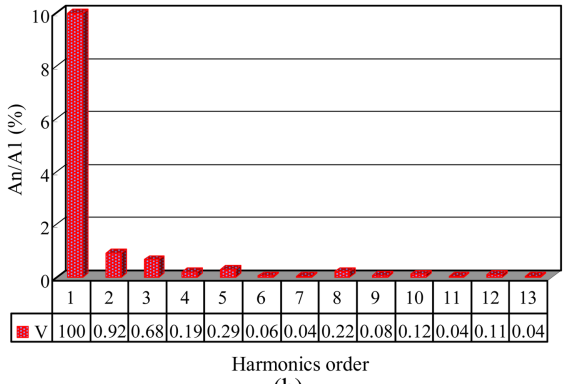

(b)

Fig. 16. (Color online) Predicted and Measured back-EMF. (a) Back-EMF waveforms. (b) Harmonics distribution of Measured back-EMF.

with the experimental result. In addition, the corresponding fundamental and harmonic components can be deduced by spectral analysis, as shown in Fig. 16(b). The A1 is the magnitude of the fundamental component and An (n = 1, 2, 3 ... 10) is the magnitude of the nth-order harmonic. It can be observed that the total harmonic distortion of the measured back-EMF waveform is 2.02 %. Fig. 17 shows the predicted and measured thrust forces. It can be shown that the results of simulation are

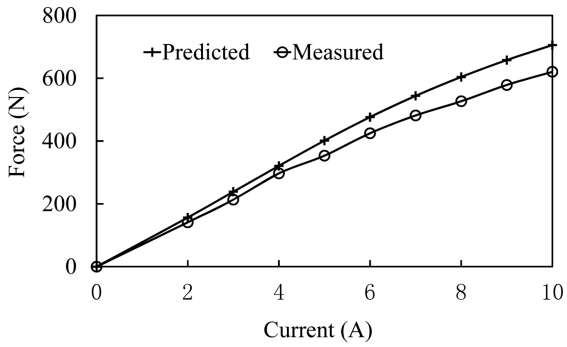

Fig. 17. (Color online) Predicted and measured thrust force versus current.

according with experiments.

6. Conclusion

In this paper, the LPMV machine with various topologies of half Halbach PM array has been designed and analyzed, which offers the high force density and low ripple. The configuration, operation principle and especially the electromagnetic performances have been studied. Based on the maximum thrust force and high resistance to demagnetization of the LPMV machine, the combinations of ratio c_w and magnetizing angle θ of the half Halbach PM array have been investigated. The results have revealed that the optimal topology of half Halbach PM array can be obtained when the values of c_w are designed as 5/9, 4/9, 1/3, 2/9 and 0, the optimal points of magnetizing angle θ are chosen as 0°, 25°, 35°, 50° and 50°, respectively. The results based on the FEM are validated to be accurate by the experiments when $c_w = 5/9$, $\theta = 0°$. The designed LPMV machine has a bright future in long stroke applications such as urban rail transits.

Acknowledgement

This work was supported in part by the National Natural Science Foundation of China (51277194 and 51422702), by the Qing Lan Project of Jiangsu Province, and by the Priority Academic Program Development of Jiangsu Higher Education Institutions.

References

[1] A. Toba and T. A. Lipo, IEEE Trans. Ind. Appl. **36**, 1539 (2000).
[2] J. Yang, G. Liu, W. Zhao, Q. Chen, Y. Jiang, L. Sun, and X. Zhu, IEEE Trans. Magn. **49**, 3826 (2013).
[3] D. Tang and J. Chang, IEEE Trans. Magn. **50**, 7021704 (2014).
[4] X. Li, K. T. Chau, and M. Cheng, IEEE Trans. Magn. **51**, 8203009 (2015).
[5] S. Jia, R. Qu, and J. Li, IEEE Trans. Magn. **51**, 8203009 (2015).
[6] L. Xu, G. Liu, W. Zhao, J. Ji, H. Zhou, W. Zhao, and T. Jiang, IEEE Trans. Magn. **30**, 1483 (2015).
[7] L. Xu, G. Liu, W. Zhao, X. Yang, and R. Cheng, IEEE Trans. Ind. Electron. **64**, 179 (2017).
[8] B. Kim and T. Lipo, IEEE Trans. Ind. Appl. **50**, 3656 (2014).
[9] D. Li and R. Qu, Proc. Int. Conf. Elect. Mach. Syst. 1 (2012).
[10] S. Niu, S. Ho, W. Fu, and L. Wang, IEEE Trans. Magn. **46**, 2032 (2010).
[11] S. Chung, J. Kim, B. Woo, D. Hong, J. Lee, and D. Koo, IEEE Trans. Magn. **47**, 4215 (2011).
[12] D. Li, R. Qu, J. Li, and W. Xu, IEEE Trans. Ind. Appl. **51**, 4470 (2015).
[13] D. Li, R. Qu, and Z. Zhu, IEEE Trans. Magn. **50**, 7019804 (2014).
[14] Y. Du, K. T. Chau, M. Cheng, Y. Fan, Y. Wang, W. Hua, and Z. Wang, IEEE Trans. Magn. **47**, 4219 (2011).
[15] Y. Du, M. Cheng, K. T. Chau, X. Liu, F. Xiao, K. Shi, and L. Mo, IEEE Trans. Magn. **50**, 4219 (2014).
[16] J. Ji, W. Zhao, Z. Fang, J. Zhao, and J. Zhu, IEEE Trans. Magn. **51**, 8106710 (2015).
[17] W. Zhao, J. Zheng, J. Wang, G. Liu, J. Zhao, and Z. Fang, IEEE Trans. Ind. Electron. **63**, 2072 (2016).
[18] Zhu, Z. Q. and D. Howe, IEEE Proc. Electr. Power. Appl. **148**, 299 (2001).
[19] Y. Shen and Z.Q. Zhu, IET Elect. Syst. Transp. **3**, 57 (2013).
[20] C. Kim and J. Choi, J. Magn. **21**, 110 (2016).
[21] Y. Du, M. Cheng, and K. T. Chau, Proc. Int. Conf. Elect. Mach. Syst. 262 (2013).
[22] S. Li, Y. Li, and B. Sarlioglu, IEEE Trans. Magn. **51**, 8106209 (2015).
[23] M. Galea, L. Papini, H. Zhang, C. Gerada, and T. Hamiti, IEEE Trans. Magn. **51**, 8107309 (2015).